

## Evidence for single particle structure of high spin states in $^{144}\text{Pm}$ and $^{145}\text{Pm}$

T. Glasmacher,\* D. D. Caussyn,<sup>†</sup> P. D. Cottle, J. W. Holcomb, T. D. Johnson,  
K. W. Kemper, M. A. Kennedy, and P. C. Womble

*Department of Physics, Florida State University, Tallahassee, Florida 32306*

(Received 29 January 1993)

Excited states of the  $Z = 61$  isotopes  $^{144}\text{Pm}_{83}$  and  $^{145}\text{Pm}_{84}$  have been studied in the  $^{19}\text{F} + ^{130}\text{Te}$  reaction at a beam energy of 85 MeV. Gamma-ray and conversion electron spectroscopy were used to establish the high spin states of  $^{144}\text{Pm}$  up to spin  $20\hbar$  and to extend the level spectrum of  $^{145}\text{Pm}$  up to a tentative spin of  $\frac{33}{2}\hbar$ . Empirical shell model calculations in a configuration space truncated to the  $\pi 1h_{11/2}$ ,  $\pi 1g_{7/2}^{-1}$ , and  $\pi 2d_{5/2}^{-1}$  protons and the  $\nu 2f_{7/2}$  neutron outside the  $^{146}\text{Gd}$  core reproduce the observed energy levels in good agreement with the experimental results.  $(\pi h_{11/2})^2$  configurations are suggested in an  $N = 83$  isotope for  $Z < 64$ .

PACS number(s): 23.20.En, 23.20.Lv, 23.20.Nx, 27.60.+j

### I. INTRODUCTION

Nuclei in the neighborhood of  $^{146}\text{Gd}$  and the  $N = 82$  shell closure are sufficiently spherical [1] to allow a single particle model description of their properties. Recently the shell model has been successfully applied to interpret the high spin states of several nuclei in this region [2–4]. A study of high spin states [5] in the  $Z = 61$  nucleus  $^{145}\text{Pm}$  provided evidence that the yrast spectrum of this nucleus can be interpreted in terms of the weak coupling of unpaired  $d_{5/2}$ ,  $g_{7/2}$ , and  $h_{11/2}$  proton holes and protons to a  $^{144}\text{Nd}$  core. This result suggests that the application of a shell model to promethium isotopes near the  $N = 82$  shell closure may be fruitful.

In this article we present the results of a study of high angular momentum states of the  $N = 83$  odd-odd nucleus  $^{144}\text{Pm}$  and its  $N = 84$  isotope  $^{145}\text{Pm}$ . Methods of  $\gamma$ -ray as well as conversion electron spectroscopy were applied to place a total of 53 transitions between 31 new levels in  $^{144}\text{Pm}$ . The level scheme extends to spin  $20\hbar$  and an excitation energy of 5.8 MeV. From our  $\gamma$ -ray information we were able to determine the  $B(E3; 9^+ \rightarrow 6^-)$  reduced transition strength in  $^{144}\text{Pm}$  which indicates that the  $9^+$  state has noncollective character. The previously published decay scheme for  $^{145}\text{Pm}$  was confirmed and three new levels as well as a few spin assignments were added. We interpret our results in terms of an empirical shell model, which uses interaction energies from adjacent nuclei. Our results allow us to test the single particle description of nuclei close to the  $N = 82$  neutron shell closure below the  $Z = 64$  shell gap.

### II. EXPERIMENTAL TECHNIQUES AND DATA ANALYSIS

The nuclei  $^{144}\text{Pm}$  and  $^{145}\text{Pm}$  were populated in the fusion evaporation reactions  $^{130}\text{Te}(^{19}\text{F}, 5n)$  and  $^{130}\text{Te}(^{19}\text{F}, 4n)$ , respectively, at a beam energy of  $E_{\text{lab}} = 85$  MeV. The fluorine beam was provided by the Florida State University FN Tandem Van de Graaff and Superconducting Linear Accelerators. Measurements of prompt and delayed  $\gamma$ - $\gamma$  coincidences,  $\gamma$ -ray angular distributions, directional correlations from oriented states (DCO ratios) and conversion electrons were performed.

For the prompt and delayed  $\gamma$ - $\gamma$  coincidence experiments a thick ( $500 \text{ mg/cm}^2$ ) self-supporting target isotopically enriched to 98.96% in  $^{130}\text{Te}$  was used. The beam energy of 85 MeV was chosen after calculations with the code PACE [6] had predicted the most favorable yield of  $^{144}\text{Pm}$  in a thick target near this energy.

During the prompt  $\gamma$ - $\gamma$  coincidence experiment four high purity germanium (HPGe) detectors, with energy resolutions between 1.9 keV and 2.1 keV (full width at half maximum) at 1.33 MeV, were each surrounded with a bismuth germanate anticoincidence shield [7] for suppression of Compton scattering background. Three of the HPGe detectors were located at  $90^\circ$  with respect to the beam direction and one HPGe detector was located at  $0^\circ$  with respect to the beam direction. The  $\gamma$ -ray singles spectrum of a  $^{152}\text{Eu}$  source placed at the target position was used to determine the energy and relative efficiency calibrations for each detector. A total of  $5 \times 10^7$   $\gamma$ - $\gamma$  coincidence events was recorded on magnetic tape for off-line analysis. The coincidence events were recalibrated to 0.75 keV/channel and sorted into a  $4096 \times 4096$  channel triangular matrix. From this array, background subtracted coincidence spectra were projected for all detected  $\gamma$ -rays. A selection of spectra for  $^{145}\text{Pm}$  is shown in Figs. 1 and 2. To determine DCO ratios, coincidences between the  $0^\circ$  detector and either of the three detectors at  $90^\circ$  were resorted into a  $2500 \times 2500$  channel square

\*Present address: National Superconducting Cyclotron Laboratory, Michigan State University, East Lansing, MI 48824.

<sup>†</sup>Present address: Indiana University Cyclotron Facility, Bloomington, IN 47405.

matrix.

Two unsuppressed HPGe detectors with energy resolutions of 2.1 keV and 2.3 keV FWHM were used in the delayed  $\gamma$ - $\gamma$ -coincidence experiment. The time between events in the two detectors was measured with a time-to-amplitude converter and  $\gamma$ - $\gamma$ -time events were written to magnetic tape for off-line analysis. A total of  $1.7 \times 10^7$  events was recorded. The data were sorted by generating a prompt and a delayed coincidence matrix. The prompt matrix contained events where the time difference between the two gamma rays is less than 30 ns while the delayed coincidence matrix contains events where the  $\gamma$  rays are between 225 and 900 ns apart. Events which were separated between 900 and 1000 ns were subtracted from both matrices to reduce the accidental background. Figure 3 shows spectra projected from the two matrices.

The angular distribution experiment was performed with two HPGe detectors. In-beam singles spectra were acquired with one detector positioned at  $0^\circ$ ,  $15^\circ$ ,  $30^\circ$ ,  $45^\circ$ ,  $60^\circ$ ,  $75^\circ$ , and  $90^\circ$  with respect to the beam direction at a distance of 23.5 cm from the target and a monitor detector fixed at  $90^\circ$  to the beam axis. The thick target was positioned at an angle of  $45^\circ$  with respect to the beam. Without beam a  $^{152}\text{Eu}$  source was attached to the front of the target and  $\gamma$ -ray singles spectra were acquired yielding an efficiency curve as a function of angle. After

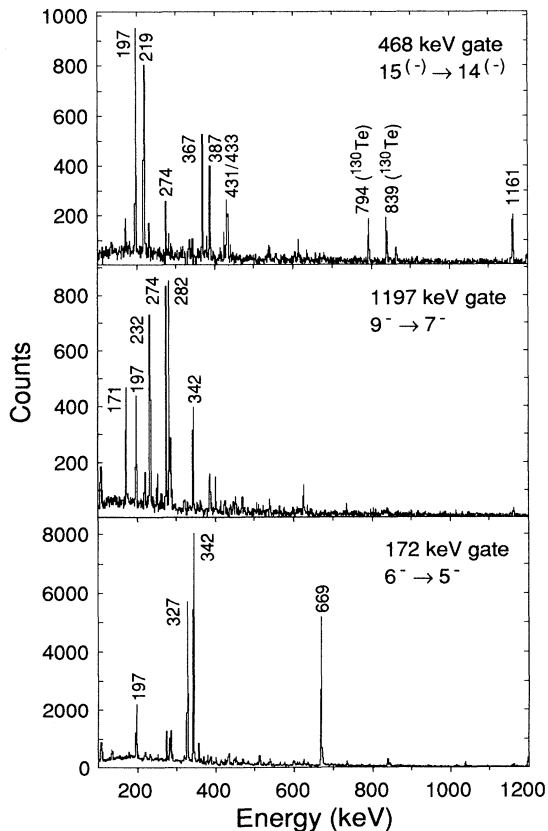


FIG. 1. Energy spectra from the  $\gamma$ - $\gamma$ -coincidence experiment gated on transitions between states of negative parity in  $^{144}\text{Pm}$ .

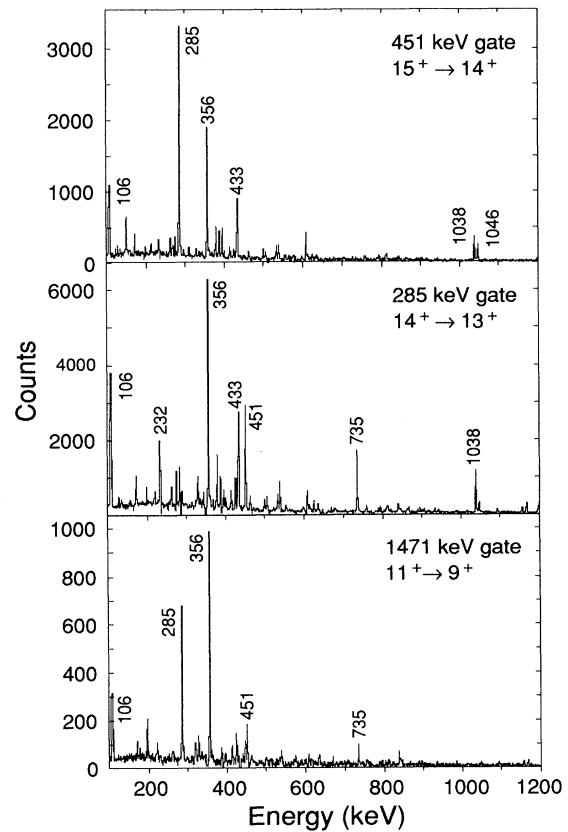


FIG. 2. Energy spectra from the  $\gamma$ - $\gamma$ -coincidence experiment gated on transitions between states of positive parity in  $^{144}\text{Pm}$ .

correcting for detector efficiency and normalizing to the monitor detector, the angular distribution of the  $\gamma$ -ray yield for each transition was fitted by the expression

$$W^{\text{exp}}(\theta) = A_0^{\text{exp}} [1 + a_2^{\text{exp}} P_2(\cos\theta) + a_4^{\text{exp}} P_4(\cos\theta)], \quad (1)$$

where the  $P_i$  are Legendre polynomials. The package PLOTDATA [8] was used to perform the fit. The best

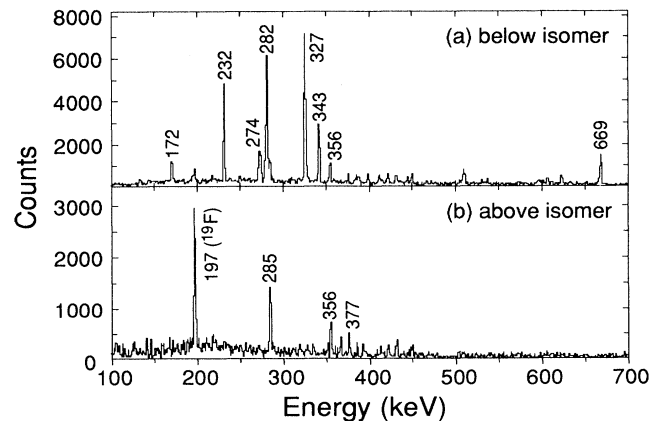


FIG. 3. Energy spectra from the delayed  $\gamma$ - $\gamma$ -coincidence experiment to identify transitions feeding the 841-keV  $9^+$  isomeric state in  $^{144}\text{Pm}$ . The time windows are explained in the text.

TABLE I. Characteristics of  $^{144}\text{Pm}$   $\gamma$  radiation.

$E_\gamma$ (keV) <sup>a</sup>	$E_i$ (keV) <sup>a</sup>	$I_\gamma$ <sup>c</sup>	$I_{tr}$ <sup>d</sup>	$a_2$	$a_4$	$R_{\text{DCO}}$	$\alpha_K$	Mult.	$\delta$	$J_i^\pi \rightarrow J_f^\pi$
55.4 <sup>f</sup>	896.5									
58.1 <sup>f</sup>	2668.3									12 <sup>+</sup> $\rightarrow$
87.1	2072.4	88(8) <sup>b</sup>						$M1^g$		11 <sup>-</sup> $\rightarrow$ 10 <sup>-</sup>
106.3	2774.6	119(7) <sup>b</sup>								13 <sup>+</sup> $\rightarrow$ 12 <sup>+</sup>
109.4	3904.5	38(2) <sup>b</sup>								$\rightarrow$ 15
127.3	2774.6	13(4) <sup>b</sup>								13 <sup>+</sup> $\rightarrow$ 12
134.4	1985.3	22(3) <sup>b</sup>								10 <sup>-</sup> $\rightarrow$ (9)
171.9	0.0	1000(60)		-0.248(83)	0.127(90)					6 <sup>-</sup> $\rightarrow$ 5 <sup>-</sup>
197.3	2269.7	187(17) <sup>b</sup>	231(21)			0.47(12)		$M1^g$	-0.011(77) <sup>h</sup>	12 <sup>-</sup> $\rightarrow$ 11 <sup>-</sup>
219.2	4118.7	87(5)	102(6)	-0.304(65)	0.108(72)		0.155(26)	$M1$		16 <sup>(-)</sup> $\rightarrow$ 15 <sup>(-)</sup>
221.0	3348.8	56(4)		-0.039(80)	0.146(92)					14 $\rightarrow$ 13
232.4	232.4	796(38)		-0.164(38)	0.040(43)					6 $\rightarrow$ 5
255.9	1711.3	38(3)		-0.09(11)	0.04(12)				0.106(74)	9 <sup>-</sup> $\rightarrow$ 8
261.6	4818.9	41(3)		-0.322(88)	-0.028(99)				-0.044(50)	18 $\rightarrow$ 17
274.0	1985.3	166(8)	182(9)	-0.267(27)	0.049(30)			$M1^j$	0.004(23)	10 <sup>-</sup> $\rightarrow$ 9 <sup>-</sup>
282.1	514.5	741(34)		-0.125(30)	0.015(35)					7 <sup>-</sup> $\rightarrow$ 6 <sup>-</sup>
283.5	3899.5	>21(2) <sup>b</sup>				0.37(16)				-0.03(14) <sup>h</sup> 15 <sup>(-)</sup> $\rightarrow$ (14)
285.4	3060.0	574(26)	624(28)	-0.171(29)	0.021(32)		0.072(10)	$M1$	0.052(18)	14 <sup>+</sup> $\rightarrow$ 13 <sup>+</sup>
288.5	3904.5	>9(2) <sup>b</sup>				0.84(20)			-0.068(93) <sup>h</sup>	$\rightarrow$ (14)
323.6	4118.7	25(3) <sup>b</sup>								16 <sup>(-)</sup> $\rightarrow$ 15
326.6	841.1	747(33)		-0.093(24)	0.000(28)					9 <sup>+</sup> $\rightarrow$ 7 <sup>-</sup>
329.8	4557.3	54(3)		-0.245(47)	0.029(54)				0.017(38)	17 <sup>+</sup> $\rightarrow$ 16
335.0	2647.3	41(3)		-0.22(10)	0.11(12)	0.45(11)			-0.027(75) <sup>h</sup>	12 $\rightarrow$ 11 <sup>+</sup>
342.6	514.5	410(25) <sup>b</sup>								7 <sup>-</sup> $\rightarrow$ 6 <sup>-</sup>
353.2	3127.8	16(3) <sup>b</sup>								13 $\rightarrow$ 13 <sup>+</sup>
356.0	2668.3	546(24)	573(25)	-0.218(23)	-0.004(25)		0.042(5)	$M1$	0.014(17)	12 <sup>+</sup> $\rightarrow$ 11 <sup>+</sup>
363.9	3795.1	22(3) <sup>b</sup>				0.55(13)			0.044(74) <sup>h</sup>	15 $\rightarrow$ 14 <sup>(-)</sup>
367.4	2072.4	169(8)		-0.322(26)	0.019(29)		<0.0136(61)	$E1$	-0.039(22)	11 <sup>-</sup> $\rightarrow$ 10 <sup>+</sup>
377.5	1274.0	259(12) <sup>b</sup>				0.465(34)				10 <sup>+</sup> $\rightarrow$
386.5	4505.2	119(5)		-0.225(12)	0.036(13)				0.030(24)	17 $\rightarrow$ 16 <sup>(-)</sup>
393.6	3904.5	28(2)		-0.575(86)	0.023(99)				-0.178(81)	$\rightarrow$ 15 <sup>+</sup>
431.0	1705.0	303(17) <sup>b</sup>				0.413(88)				10 <sup>+</sup> $\rightarrow$ 10 <sup>+</sup>
432.9	1274.0	497(22)	511(23)	0.289(12)	-0.061(15)		> 0.0251(39)	$M1/E2$	0.249(8)	10 <sup>+</sup> $\rightarrow$ 9 <sup>+</sup>
446.5	3795.1	137(7)		-0.242(32)	-0.045(36)					15 $\rightarrow$ 14
450.9	3510.9	175(8)	180(8)	-0.068(22)	0.097(25)		0.0255(30)	$M1$		15 <sup>+</sup> $\rightarrow$ 14 <sup>+</sup>
459.5	3127.8	43(2)		-0.102(91)	0.038(11)					13 $\rightarrow$ 12 <sup>+</sup>
462.3	2774.6	40(2)	41(2)	0.178(33)	-0.091(42)		<0.0285(83)	$E2$	-0.088(40)	13 <sup>+</sup> $\rightarrow$ 11 <sup>+</sup>
468.3	3899.5	91(4)	93(4)	-0.090(35)	-0.001(42)	0.532(66)	0.0177(64)	$M1$	0.087(29)	15 <sup>(-)</sup> $\rightarrow$ 14 <sup>(-)</sup>
499.0	5850.6	32(2)		-0.261(65)	0.030(78)				0.017(32)	20 $\rightarrow$ 19
504.9	2774.6	41(2)	41(2)	-0.172(39)	-0.046(46)			$E1$	0.022(53)	13 <sup>+</sup> $\rightarrow$ 12 <sup>-</sup>
532.7	5351.6	37(2)		-0.137(50)	-0.013(61)				0.077(44)	19 $\rightarrow$ 18
574.2	3348.8	60(4)		-0.159(53)	0.009(65)				0.054(30)	14 $\rightarrow$ 13 <sup>+</sup>
607.8	4118.7	96(6) <sup>b</sup>								16 <sup>(-)</sup> $\rightarrow$ 15 <sup>+</sup>
613.6	5118.8	32(2)		0.074(76)	-0.095(96)					
624.9	2610.2	43(5) <sup>b</sup>								$\rightarrow$ 10 <sup>-</sup>
669.2	841.1	341(30) <sup>b</sup>	345(30) <sup>e</sup>							9 <sup>+</sup> $\rightarrow$ 6 <sup>-</sup>
735.1	3795.1	160(10) <sup>b</sup>								15 $\rightarrow$ 14 <sup>+</sup>
794.3	5351.6	81(7) <sup>b</sup>								19 $\rightarrow$ 17 <sup>+</sup>
839.5	3899.5	24(7) <sup>b</sup>								15 <sup>(-)</sup> $\rightarrow$ 14 <sup>+</sup>
863.9	1705.0	115(5)	116(5)	0.201(33)	-0.036(42)		0.0058(15)	$M1/E2$	0.252(10)	10 <sup>+</sup> $\rightarrow$ 9 <sup>+</sup>
942.3	2647.3	57(3)		0.246(26)	-0.122(32)				-0.068(46)	12 $\rightarrow$ 10 <sup>+</sup>
1038.3	2312.3	487(22)	489(22)	0.223(27)	-0.099(34)		0.0026(4)	$M1/E2$	0.233	11 <sup>+</sup> $\rightarrow$ 10 <sup>+</sup>
1046.4	4557.3	72(3)	72(3)	0.260(40)	-0.199(52)			$E2^i$	-0.070(25)	17 <sup>+</sup> $\rightarrow$ 15 <sup>+</sup>
1161.5	3431.2	132(6)	132(6)	0.284(27)	-0.214(36)				-0.084(22)	14 <sup>(-)</sup> $\rightarrow$ 12 <sup>(-)</sup>
1167.5	4227.5	69(3)		0.263(46)	-0.222(58)			$E2^i$	-0.091(43)	16 $\rightarrow$ 14 <sup>+</sup>
1196.8	1711.3	166(7)	166(7)	0.200(14)	-0.139(18)				-0.108(31)	9 <sup>-</sup> $\rightarrow$ 7 <sup>-</sup>
1223.0	1455.4	21(3)		0.19(16)	-0.23(20)					8 $\rightarrow$ 6 <sup>-</sup>
1336.2	2610.2	49(8) <sup>b</sup>								$\rightarrow$ 10 <sup>+</sup>
1336.4	1850.9	62(4) <sup>b</sup>								(9) $\rightarrow$ 7 <sup>-</sup>
1346.3	3616.0	53(4) <sup>b</sup>								(14) $\rightarrow$ 12 <sup>-</sup>
1471.2	2312.3	231(10)	231(10)	0.269(23)	-0.195(31)			$E2^j$	-0.089(19)	11 <sup>+</sup> $\rightarrow$ 9 <sup>+</sup>

<sup>a</sup>Energies are accurate to 0.1 keV.<sup>b</sup>Intensities from coincidence data (85 MeV).<sup>c</sup> $\gamma$ -ray intensities relative to 171.9-keV  $\gamma$ -ray intensity.<sup>d</sup>Intensity (including internal conversion) relative to 171.9-keV  $\gamma$ -ray intensity.<sup>e</sup>Assuming mixing ratio  $\delta = 0$ .<sup>f</sup>Not observed since outside the energy detection range.<sup>g</sup>From intensity balance.<sup>h</sup>From DCO ratio measurement.<sup>i</sup>From transition rate estimate.<sup>j</sup> $\Pi_i$  and  $\Pi_f$  known.

TABLE II. Characteristics of  $^{145}\text{Pm}$   $\gamma$  radiation at 85-MeV beam energy.

$E_\gamma$ (keV) <sup>a</sup>	$E_i$ (keV) <sup>a</sup>	$I_\gamma$ <sup>c</sup>	$I_{\text{tr}}$ <sup>d</sup>	$a_2$	$a_4$	$R_{\text{DCO}}$	$\delta$	$J_i^\pi \rightarrow J_f^\pi$
253.4	4014.1	109(10) <sup>b</sup>		-0.306(43)	0.084(48)		-0.020(16)	$\frac{31}{2} \rightarrow \frac{29}{2}$
263.2	3760.7	115(9) <sup>b</sup>		-0.236(61)	0.039(69)		0.008(44)	$\frac{29}{2} \rightarrow \frac{27}{2}$
311.7	4701.7	104(18) <sup>b</sup>		-0.212(29)	0.035(33)		0.017(32)	$(\frac{33}{2}) \rightarrow (\frac{31}{2})$
444.9	3497.5	108(22) <sup>b</sup>				1.12(7)	-0.07(12) <sup>e</sup>	$\frac{27}{2} \rightarrow \frac{27}{2}$
622.0	2124.8	75(10)	76(10)			1.03(15)	0.035(86) <sup>e</sup>	$\frac{19}{2}(+) \rightarrow \frac{15}{2}+$
708.0	3760.7	315(22) <sup>b</sup>				0.39(4)	-0.060(31) <sup>e</sup>	$\frac{29}{2} \rightarrow \frac{27}{2}$
711.2	3160.1	60(5) <sup>b</sup>		0.281(68)	-0.042(86)	1.10(14)	0.305(68)	$\frac{25}{2} \rightarrow \frac{23}{2}$
853.5	3665.3	83(14) <sup>b</sup>		0.292(44)	-0.183(57)			$\frac{27}{2} \rightarrow \frac{23}{2}(+)$
1171.5	4224.2	145(10) <sup>b</sup>		0.22(12)	-0.24(15)			$\frac{31}{2} \rightarrow \frac{27}{2}$
1337.3	4390.0	41(3) <sup>b</sup>						$\frac{31}{2} \rightarrow \frac{27}{2}$

<sup>a</sup>Energies are accurate to 0.1 keV.

<sup>b</sup>Intensities from coincidence data (75 MeV) reported in [5].

<sup>c</sup> $\gamma$ -ray intensities relative to 653.2-keV  $\gamma$ -ray intensity reported in [5].

<sup>d</sup>Intensity (including internal conversion) relative to 653.2-keV  $\gamma$ -ray intensity.

<sup>e</sup>From DCO ratio measurement.

fits for  $a_2^{\text{exp}}$  and  $a_4^{\text{exp}}$  are given in Tables I and II. The errors are quoted at the  $1\sigma$  level. Figure 4 shows typical angular distributions in  $^{144}\text{Pm}$ . Angular distributions could be measured for transitions above an energy of 120 keV only, since photons of lower energy were absorbed by the tantalum target backing.

The angular distribution data were used to obtain information on spin assignments, mixing ratios  $\delta$  (defined according to [9]), and the alignment of the magnetic sub-

states, which was assumed to follow a Gaussian distribution with width  $\sigma$ . It was also assumed that all transitions placed in the decay scheme were dipole, quadrupole, or octupole in nature and that only the lowest two multipoles allowed by the selection rules were present in a transition.

For each transition for which a  $\gamma$ -ray angular distribution was measured and the spin  $J_f$  for the final state was known, the function

$$\chi^2(J_i, J_f) = \frac{1}{6} \sum_{i=1}^7 \left( \frac{A_0^{\text{exp}}[1 + a_2^{\text{th}}(\sigma, \delta)P_2(\cos\theta_i) + a_4^{\text{th}}(\sigma, \delta)P_4(\cos\theta_i)] - W^{\text{exp}}(\theta_i)}{\Delta W^{\text{exp}}(\theta_i)} \right)^2 \quad (2)$$

was minimized with respect to  $\delta$  and  $\sigma$  for all possible spins of the initial state,  $J_i$ . For transitions in  $^{145}\text{Pm}$  the width  $\sigma$  of the Gaussian distribution, describing the alignment of the magnetic substates [9], was fixed to  $\sigma/J_i = 0.274$  to be consistent with results reported in [5]. For transitions in  $^{144}\text{Pm}$  it was found in a free fit, which allowed the variation of  $\delta$  as well as of  $\sigma/J_i$ , that the alignment of the magnetic substates depends roughly linearly on the spin of the initial state  $J_i$ , namely

$$\sigma/J_i = 0.407 - 0.016 J_i. \quad (3)$$

The mixing ratios listed in Tables I and II result from a minimization of  $\chi^2$  [given in Eq. (2)] with  $\sigma$  fixed to the values given above. Mixing ratios are quoted if only one value  $\delta$  is within the 50% confidence limit. The errors are given at the  $1\sigma$  level. Plots of  $\chi^2$  vs  $\arctan(\delta)$  for two transitions are shown in Fig. 5.

Where angular distribution information is available, the  $\gamma$ -ray intensities,  $I_\gamma$ , are taken to be the best fit for  $A_0^{\text{exp}}$  in Eq. (1). If the  $\gamma$ -rays were too weak in the singles spectra or in the presence of  $\gamma$ -ray doublets, the intensities were taken from coincidence data. Intensities are listed in Tables I and II. The total transition strength,  $I_{\text{Tr}}$ , was determined from  $I_{\text{Tr}} = (1 + \alpha)I_\gamma$ , where the total conversion coefficient  $\alpha$  was calculated from

$$\alpha = \frac{\alpha(L) + \delta^2 \alpha(L+1)}{1 + \delta^2} \quad (4)$$

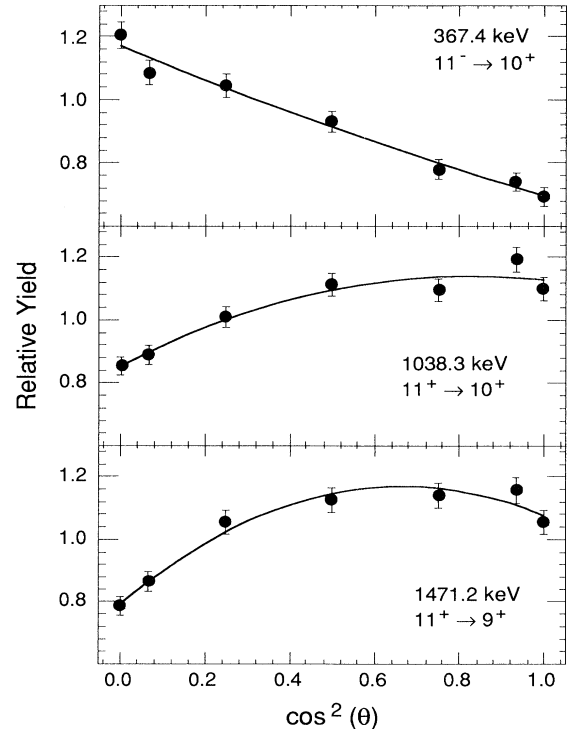


FIG. 4. Angular distributions for selected  $\gamma$ -rays in  $^{144}\text{Pm}$ . The solid curves are the Legendre polynomial fits described in the text.

for a mixed transition of multipolarity  $(L + 1)/L$  with mixing ratio  $\delta$ . Theoretical values [10] were used for the total conversion coefficients  $\alpha(L)$  and  $\alpha(L + 1)$ .

For some transitions which were too weak to be identified in the angular distribution singles spectra it was possible to measure directional correlations (of  $\gamma$  radiation) from oriented states (DCO ratios) in the  $\gamma$ - $\gamma$ -coincidence experiment. For the geometry used in our experiment the experimental DCO ratio for a photon  $\gamma_1$  is defined as the ratio of intensities

$$R_{\text{DCO}} = \frac{I(\gamma_1 \text{ obs. at } 0^\circ, \text{ gated by } \gamma \text{ obs. at } 90^\circ)}{I(\gamma_1 \text{ obs. at } 90^\circ, \text{ gated by } \gamma \text{ obs. at } 0^\circ)}. \quad (5)$$

The experimentally determined DCO ratios are presented in Tables I and II. Theoretical values for different spin combinations and mixing ratios were calculated, following the procedure given in [11]. A comparison between experimental and theoretical DCO ratios helped with the assignment of spins and allowed the determination of mixing ratios in a few cases.

During the conversion electron experiment both  $\gamma$ -ray and conversion electron singles spectra were collected, parts of which are shown in Fig. 6. A thin target of 400  $\mu\text{g}/\text{cm}^2$  of  $^{130}\text{Te}$  (isotopically enriched to 99.29%) evaporated onto a 50  $\mu\text{g}/\text{cm}^2$  carbon foil was used. The  $\gamma$  rays were detected with a HPGe detector with a resolution of 2.1 keV FWHM at 1.33 MeV. The HPGe detector was located approximately 20 cm from the target at an

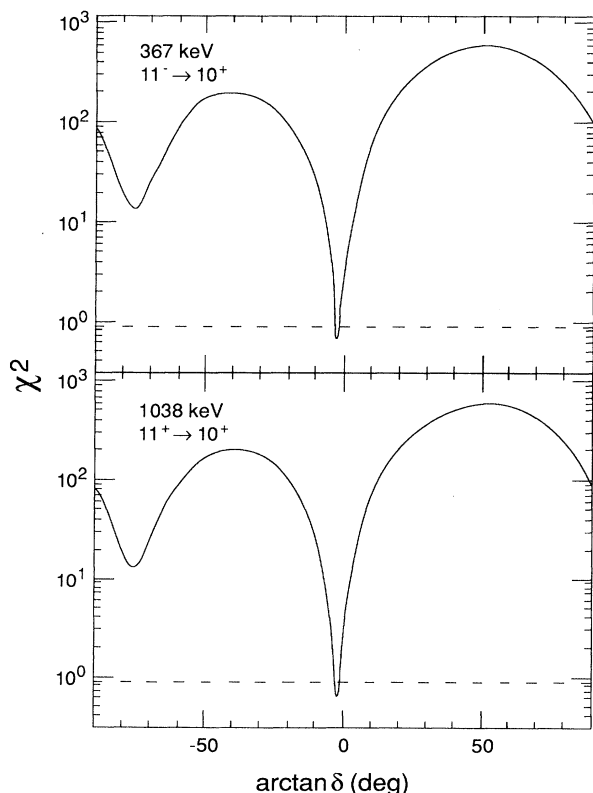


FIG. 5. The goodness-of-fit  $\chi^2$  (given in [5]) as a function of the mixing ratio  $\delta$  for two transitions in  $^{144}\text{Pm}$ . The dashed line indicates the 50% confidence limit.

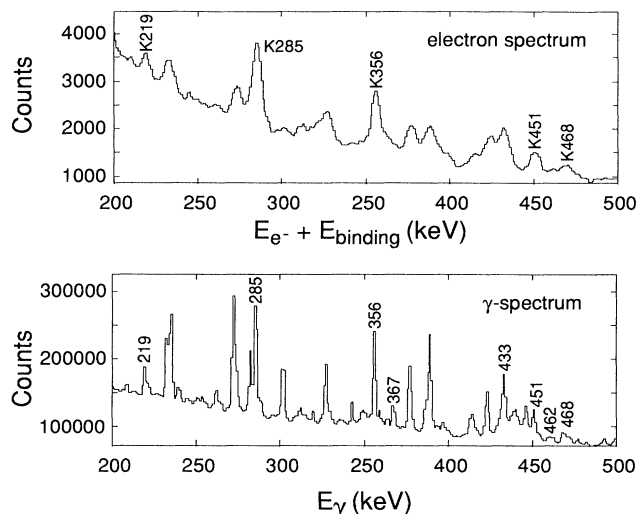


FIG. 6. Portions of the  $\gamma$ -ray and electron spectra from the electron conversion measurement. The energy scale of the electron spectrum is shifted by the  $K$ -electron binding energy of promethium ( $E_{\text{binding}} = 45.2$  keV).

angle of  $90^\circ$  to the beam direction. Conversion electrons were detected with a miniorange electron spectrometer that included a liquid-nitrogen-cooled Si(Li) detector of 5 mm thickness and 1 cm diameter. The magnetic filter, similar to that described by van Klinken and Wisshak [12] and Ishi [13], consisted of five thin, flat permanent magnets placed around a central lead plug which shielded the detector from direct exposure to the target. In source experiments the spectrometer yielded an energy resolution of 3.5 keV at 500 keV, while the resolution in beam was 5.0 keV at 500 keV due to kinematic broadening of the electron peaks. The relative efficiencies of the two detectors were measured with open  $^{152}\text{Eu}$  and  $^{207}\text{Bi}$  sources.

For a specific transition a conversion coefficient was determined by multiplying the ratio of the yield of conversion electrons to the yield of  $\gamma$ -rays, with each yield corrected for the detectors' relative efficiencies, by a nor-

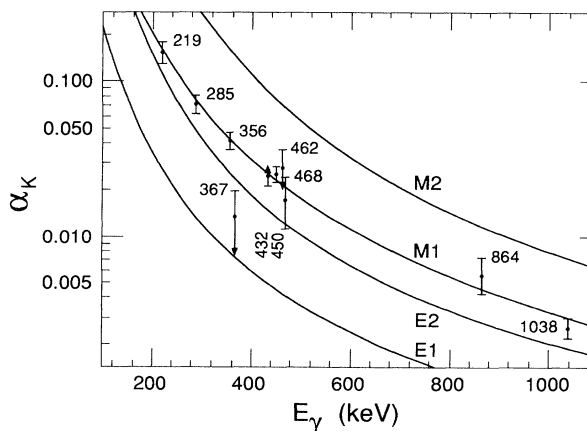


FIG. 7. Comparison of measured electron conversion coefficients in  $^{144}\text{Pm}$  with theoretical [15] values for different multipolarities.



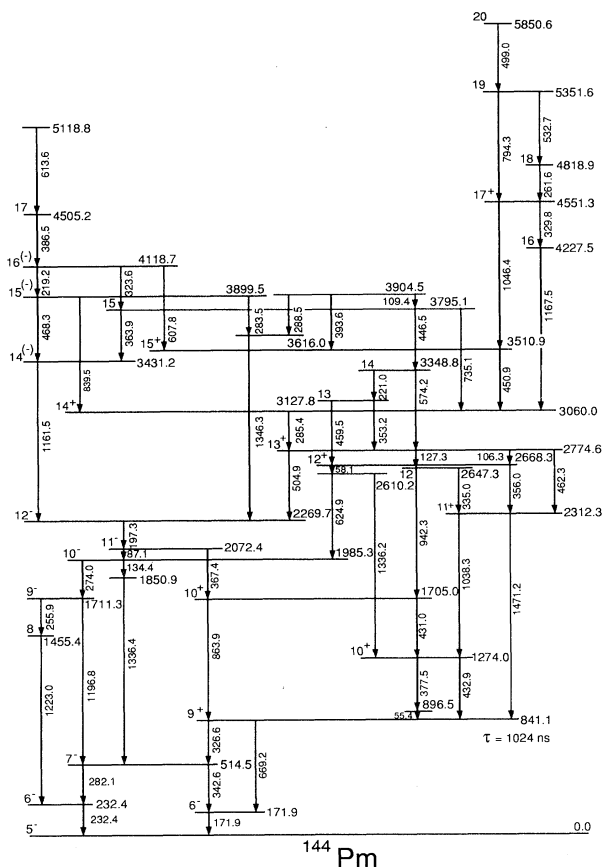


FIG. 9. Decay scheme of high spin states in  $^{144}\text{Pm}$  as deduced in this work.

meric state at 841 keV. A selection of prompt coincidence energy spectra in  $^{144}\text{Pm}$  gated on transitions in the negative parity cascade is shown in Fig. 1 and gates in the positive parity cascade are given in Fig. 2.

The 433-keV transition feeding the  $9^+$  isomer at 841 keV is a  $\Delta J = 1$  mixed  $M1/E2$  transition and thus establishes spin and parity  $J^\pi = 10^+$  for the state at 1274 keV. The 1038-keV transition going into the 1274-keV state is also  $M1/E2$  in character; therefore the 2312-keV state has  $J^\pi = 11^+$ . This spin assignment is consistent with the angular distribution of the 1471-keV transition (Fig. 4), which is characteristic of a stretched quadrupole transition. The  $M1$  character of the 356-keV transition allows the assignment of spin and parity  $J^\pi = 12^+$  to the state at 2668 keV.

The state at 2775 keV was assigned  $13^+$  because the angular distribution of the 462-keV transition connecting it to the 2312-keV  $11^+$  state is consistent with it being a stretched quadrupole and the upper limit on its conversion coefficient excludes the possibility of it having  $M2$  character. The positive parity assignment for the 2775-keV state is also supported by an intensity argument. If the 106-keV transition is  $E1$ , the total intensity of all the transitions deexciting the 2775-keV state would not be large enough to balance the intensities of the feeding transitions. [The total conversion coefficients for a 106-

keV transition in promethium are  $\alpha(E1) = 0.226$  and  $\alpha(M1) = 1.324$ .]

The mixed  $M1/E2$  character of both the 285-keV and the 451-keV transitions allows us to assign spins and parities to the levels at 3060 keV ( $14^+$ ) and 3511 keV ( $15^+$ ). The angular distribution results allow the assignments of spins to the states at 4228 keV, 4551 keV, 4819 keV, 5352 keV, and 5851 keV. Positive parity can be assigned to the 4551-keV ( $17^+$ ) state for the following reason: The 4551-keV state is being deexcited by two competing transitions, 1046 keV and 330 keV in energy. If the 1046-keV transition had  $M2$  multipolarity its slow transition rate [which would be  $(1.30 \text{ ns})^{-1}$  if it has the upper recommended value by *Nuclear Data Sheets* of 1 W.u. for the  $M2$  transition strength] could not compete with the 330 keV dipole transition. Therefore, the 1046-keV transition must be  $E2$ .

The 460-keV, 574-keV, and 447-keV transitions are stretched dipoles and thus allow the assignment of spins to the states at 3128 keV, 3349 keV, and 3795 keV.

From the  $M1/E2$  character of the 864-keV transition the state at 1705 keV can be assigned  $J^\pi = 10^+$ . With the 367-keV transition being a stretched electric dipole we find  $J^\pi = 11^-$  for the level at 2072 keV. The 1711-keV state can be assigned spin  $J = 9$  from the angular distribution information of the 1197-keV transition. If this transition is a magnetic quadrupole its slow transition rate [which can be estimated to be  $(0.66 \text{ ns})^{-1}$  using the upper recommended value by *Nuclear Data Sheets* of 1 W.u. for the  $M2$  transition strength] could not compete with the 256-keV transition. Therefore, the 1197-keV transition must be  $E2$  which allows the assignment of  $J^\pi = 9^-$  to the state at 1711 keV.

The 1985-keV state is assigned spin  $J = 10$  on the basis of the angular distribution for the 274-keV transition and negative parity because the 87-keV transition must be  $M1/E2$  in order to balance intensities in the 2072-keV state. The 2270-keV state can be assigned spin  $J = 12$  from the stretched dipole character of the 505-keV transition. This assignment is consistent with the DCO ratio of the 197-keV transition. No conversion electron or angular distribution information is available for the 197-keV transition, since it is a doublet with a ground state transition in  $^{19}\text{F}$ , and inelastic scattering of the beam produces a significant  $\gamma$ -ray yield in singles. In order to balance intensities in the 2270-keV state the 197-keV transition must be  $M1$ ; thus the 2270-keV state has negative parity. The angular distribution for the 1161-keV transition shows that it is a stretched quadrupole, therefore we assign a spin of  $J = 14$  to the state at 3431 keV. No firm parity assignment can be made for this state; however, a tentative negative parity assignment is given because  $M2$  character would make the 1161-keV transition relatively slow. However, this possibility cannot be excluded with the current experimental data. The assignments for the states at 3900 keV ( $15^-$ ), 4119 keV ( $16^-$ ), and 4505 keV ( $17^-$ ) follow from angular distribution and conversion coefficient information for the connecting transitions.

From the previously reported lifetime of the  $9^+$  isomer [17] of  $\tau = 1024$  ns and the branching ratios of the 669-keV and the 327-keV transitions deexciting the 841-

TABLE III. Efficiency corrected intensities and strength of transitions below the  $9^+$  isomer in  $^{144}\text{Pm}$ .

Energy (keV)	Intensity (arb. units)	Relative intensity (%)	Reduced transition strength (W.u.)
326.6	747(33)	68.4(42)	$B(M2) = 0.29(2)$
669.2	345(30)	31.6(31)	$B(E3) = 3.24(71)$
	1092(46)	100	

keV state, reduced transition matrix elements were determined. The intensities are taken from a spectrum formed by summing energy gates on the 423-keV, 1471-keV, and 1038-keV transitions and they are presented in Table III. The errors quoted are due to uncertainties in the intensities only and do not include an error for the lifetime of the isomer. Our reduced transition matrix elements of  $B(E3; 9^+ \rightarrow 6^-) = 3.24(71)$  W.u. and  $B(M2, 9^- \rightarrow 7^-) = 0.29(2)$  W.u. differ from the previously reported ones [17]  $B(E3) = 10.5$  W.u. and  $B(M2) = 0.19$  W.u. In [17] a branching ratio of 49% and 51% for the 327-keV and the 669-keV transitions was assumed, respectively; however, the branching ratio in [17] was not measured but deduced from compiled intensities.

## V. EMPIRICAL SHELL MODEL CALCULATIONS

Nuclei with 82 neutrons have long been successfully described by the shell model [18]. With the discovery of the  $Z = 64$  subshell closure [19] it became possible to discuss properties of nuclei near  $^{146}\text{Gd}$  in terms of a small number of valence protons or proton holes. Even though the proton-shell closure becomes less pronounced when neutrons are coupled to the  $Z = 64$ ,  $N = 82$  core [20],  $Z = 64$  nuclei remain spherical for  $N < 86$  and do not become well deformed until  $N \geq 90$  [1]. As a result, a shell-model-like description is possible for nuclei close to the  $N = 82$  shell closure. Yrast levels at moderately high and high spins are especially well suited for an analysis in the framework of the shell model since they are preferably formed by near fully and fully aligned multi-particle configurations yielding close to pure shell model configurations.

While conventional shell model calculations determine the interaction between particles from a given potential, an alternative approach, first suggested by Talmi [21], uses empirical interaction energies from adjacent nuclei. This approach has been applied in the gadolinium region [2–4, 22, 23]. These calculations, called empirical shell model calculations, allow the decomposition of a nuclear state into substructures corresponding to specific levels in neighboring nuclei. The energy  $E(\Psi, N)$  of a state  $\Psi$  in a nucleus  $N$  relative to a closed core, here  $^{146}\text{Gd}$ , is expressed in terms of the single particle energies  $E_{s.p.}(\Psi, N)$  and interaction energies  $\langle(\Psi, N)\rangle$  of the orbits involved, namely  $E(\Psi, N) = E_{s.p.}(\Psi, N) + \langle(\Psi, N)\rangle$ . To express this energy  $E(\Psi, N)$  as an excitation energy  $E_x(\Psi, N)$  in the nucleus  $N$ , the ground state mass of the nucleus  $N$ ,  $E_{g.s.}(N)$ , relative to the  $^{146}\text{Gd}$  core, must be subtracted, thus  $E_x(\Psi, N) = E(\Psi, N) - [E_{g.s.}(N) - E_{g.s.}(^{146}\text{Gd})]$ .

TABLE IV. Experimental single particle energies in the  $^{146}\text{Gd}$  region. Each state is labeled by its predominant configuration and its energy relative to the  $^{146}\text{Gd}$  core.

Nucleus	Excitation energy (keV)	Orbit	Single particle energy (keV)
$^{145}_{63}\text{Eu}^a$	0	$\pi 2d_{5/2}^{-1} \equiv d$	5366
$^{145}_{63}\text{Eu}^a$	330	$\pi 1g_{7/2}^{-1} \equiv g$	5696
$^{147}_{65}\text{Tb}^c$	51	$\pi 1h_{11/2} \equiv h$	-1906
$^{147}_{64}\text{Gd}^b$	0	$\nu 2f_{7/2} \equiv f$	-7339

<sup>a</sup>Mass excess taken from Blomqvist *et al.* [24].

<sup>b</sup>Mass excess taken from Wapstra *et al.* [26].

<sup>c</sup>Mass excess taken from Rubio *et al.* [25].

Ground state masses were calculated from tabulated values for the mass excesses of the respective nuclei, which were taken from Blomqvist *et al.* [24], Rubio *et al.* [25], and Wapstra *et al.* [26] as indicated in Table V. The ground state masses for  $^{144,145}\text{Pm}$  were calculated using mass excess values from [26].

Empirical single particle energies were obtained from one-valence particle nuclei relative to the  $^{146}\text{Gd}$  core and they are listed in Table IV. The interaction energies were extracted from states with related configurations in neighboring nuclei or, where such states were not available, recoupled using angular momentum algebra [27] from two-body interaction energies. Two-particle interaction energies in the gadolinium region have been compiled by Piiparinen *et al.* [3] (mainly for  $Z < 64$ ) and by Kuhnert *et al.* [4] (for  $Z > 64$ ). While a complete decomposition of the interaction energy of a given configuration into two-body matrix elements is always possible, it is sometimes more convenient and more advantageous to decompose it into terms representing more than two particles. The interaction terms are then more closely related to the final configuration than the two-body interactions are, and effects such as configuration mixing and core polarization are to some extent automatically included. The present calculations do not explicitly take configuration mixing into account; the interaction energies used are listed in Table V.

## VI. CONFIGURATIONS FOR $^{145}\text{Pm}$

The theoretical energy levels for  $^{145}\text{Pm}$ , presented in Fig. 10, have been calculated from the single particle energies given in Table IV and the interaction energies given in Table V. The calculations were made under the simplifying assumption that pairs of identical particles couple to the lowest possible spin for each configuration.

Core states in  $^{142}\text{Nd}$  are denoted in Figs. 10 and 11 by  $j_L^{-4}$ , where  $L$  is the spin to which the four holes are coupled, since they have mixed shell model configurations involving  $d$  and  $g$  protons [18, 28, 29]. For the calculation of interaction matrix elements involving these core states (listed in Table V) single particle energies of the  $d$  proton are used.

States of odd parity in  $^{145}\text{Pm}$  are built on top of the  $\frac{1}{2}^-$  isomer. The structure of this isomer involves the

TABLE V. Residual interaction energies used in the empirical shell model calculations. The proton orbitals  $\pi 2d_{5/2}^{-1}$ ,  $\pi 1g_{7/2}^{-1}$ , and  $\pi 1h_{11/2}$  are abbreviated  $d^{-1}$ ,  $g^{-1}$ , and  $h$ , while  $f$  represents the  $\nu 2f_{7/2}$  neutron orbit. The symbol  $j^{-4}$  stands for core states in  $^{142}\text{Nd}$ . All energies are given in keV;  $E_x$  is the energy of the observed level in the nucleus of interest and  $E$  is this energy with respect to the  $^{146}\text{Gd}$  core. Energies estimated by scaling from other mass regions are given in *italics*.

Nucleus	Configuration	Spin	$E_x$	$E$	$\Delta_{\text{int}}$	Ref.	Nucleus	Configuration	Spin	$E_x$	$E$	$\Delta_{\text{int}}$	Ref.	
$^{141}_{59}\text{Pr}^{\text{b}}$	$\pi j_0^{-4} d^{-1}$	5/2 <sup>+</sup>	0	26518	-312	[38]	$^{145}_{62}\text{Sm}^{\text{b}}$	$\pi d^{-2} \nu f$	7/2 <sup>-</sup>	0	1946	-1447	[3]	
$^{142}_{60}\text{Nd}^{\text{b}}$	$\pi j^{-4}$	0 <sup>+</sup>	0	19295	-2169	[39]			11/2 <sup>-</sup>	1538	3484	91	[47]	
		2 <sup>+</sup>	1576	20871	-593	[39]			13/2 <sup>-</sup>			594	<sup>d</sup>	
		4 <sup>+</sup>	2101	21396	-68	[39]			15/2 <sup>-</sup>			762	<sup>d</sup>	
	$\pi d^{-3} g^{-1}$	6 <sup>+</sup>	2209	21504	-290	[39]		$\pi d^{-1} g^{-1} \nu f$	19/2 <sup>-</sup>	2711	4657	934	[3]	
		8 <sup>+</sup>	3453	22748	954	[39]		$\pi g_6^{-2} \nu f$	19/2 <sup>-</sup>			1300	<sup>d</sup>	
	$\pi g^{-4}$	6 <sup>+</sup>	2887	22182	-690	[39]	$^{146}_{62}\text{Sm}^{\text{b}}$	$\pi d^{-2} \nu f^2$	0 <sup>+</sup>	0	-6466	-2520	[48]	
$^{143}_{60}\text{Nd}^{\text{b}}$	$\pi j^{-4} \nu f$	7/2 <sup>-</sup>	0	13172	-953	[40]			2 <sup>+</sup>	747	-5719	-1773	[48]	
		11/2 <sup>-</sup>	1431	14603	478	[41]			4 <sup>+</sup>	1381	-5085	-1139	[48]	
		13/2 <sup>-</sup>	2067	15239	1114	[42]			6 <sup>+</sup>	1812	-6466	-708	[48]	
		15/2 <sup>-</sup>	2019	15191	1066	[40]			8 <sup>+</sup>	2737	-3729	217	[48]	
	$\pi g^{-4} \nu f$	17/2 <sup>-</sup>	2398	15570	125	[40]			10 <sup>+</sup>	3775	-2691	1255	[48]	
		19/2 <sup>-</sup>	2490	15662	217	[40]			8 <sup>+</sup>	3043	-3423	-137	[48]	
								10 <sup>+</sup>	3775	-2691	595	[48]		
$^{144}_{60}\text{Nd}^{\text{b}}$	$\pi j_0^{-4} \nu f^2$	0 <sup>+</sup>	0	5354	-1432	[43]	$^{145}_{63}\text{Eu}^{\text{a}}$	$\pi h d_0^{-2}$	11/2 <sup>-</sup>	716	6082	-2744	[49]	
		2 <sup>+</sup>	696	6050	-736	[43]		$\pi h g_0^{-2}$	15/2 <sup>-</sup>	2284	7650	-1176	[49]	
		4 <sup>+</sup>	1314	6668	-118	[43]		$\pi h d_4^{-2}$	15/2 <sup>-</sup>	2574	7940	-886	[49]	
	$\pi j^{-4} \nu f_6^2$	6 <sup>+</sup>	1791	7145	359	[43]			17/2 <sup>-</sup>	2814	8180	-646	[47]	
		8 <sup>+</sup>	2709	8063	1277	[43]			19/2 <sup>-</sup>	2863	8229	-597	[49]	
		10 <sup>+</sup>	3574	8928	2142	[43]			23/2 <sup>-</sup>	3183	8549	-607	[49]	
						$^{146}_{63}\text{Eu}^{\text{a}}$	$\pi d^{-1} \nu f$	4 <sup>-</sup>	0	-1881	92	[2]		
$^{143}_{61}\text{Pm}^{\text{b}}$	$\pi d^{-1} g^{-2}$	9/2 <sup>+</sup>			416	<sup>d</sup>			5 <sup>-</sup>	14	-1867	106	[2]	
		13/2 <sup>+</sup>			550	<sup>d</sup>			6 <sup>-</sup>	289	-1592	381	[2]	
		17/2 <sup>+</sup>	2288	17284	526	[28]			5 <sup>-</sup>	316	-1565	78	[2]	
	$\pi d^{-2} g^{-1}$	17/2 <sup>+</sup>			668	<sup>d</sup>			6 <sup>-</sup>	373	-1508	135	[2]	
		7/2 <sup>+</sup>	272	15268	-1160	[28]		$\pi g^{-1} \nu f$	7 <sup>-</sup>	648	-1233	410	[2]	
		11/2 <sup>+</sup>	1663	16659	231	[28]			6 <sup>-</sup>	373	-1508	135	[2]	
	$\pi d^{-3}$	13/2 <sup>+</sup>	1951	16947	519	[28]			7 <sup>-</sup>	648	-1233	410	[2]	
		15/2 <sup>+</sup>	1898	16894	466	[28]			7 <sup>-</sup>	648	-1233	410	[2]	
		5/2 <sup>+</sup>	0	14996	-1102	[28]			6 <sup>-</sup>	373	-1508	135	[2]	
	$\pi j^{-4} h$	9/2 <sup>+</sup>	1260	16256	158	[28]			7 <sup>-</sup>	648	-1233	410	[2]	
		11/2 <sup>-</sup>	960	15956	-3602	[28]		$^{147}_{63}\text{Eu}^{\text{b}}$	$\pi d^{-1} \nu f_0^2$	5/2 <sup>+</sup>	0	-10310	-998	[50]
		13/2 <sup>-</sup>	1951	16947	-2611	[44]			$\pi d^{-1} \nu f_2^2$	9/2 <sup>+</sup>	776	-9534	-222	[51]
	15/2 <sup>-</sup>	2437	17433	-2125	[28]			$\pi d^{-1} \nu f_4^2$	13/2 <sup>+</sup>	1421	-8889	423	[51]	
	17/2 <sup>-</sup>	2882	17878	-1680	[44]			$\pi d^{-1} \nu f_6^2$	17/2 <sup>+</sup>	1833	-8477	835	[51]	
	19/2 <sup>-</sup>	2930	17926	-1632	[28]			$\pi g^{-1} \nu f_2^2$	11/2 <sup>+</sup>	1034	-9276	-294	[51]	
	21/2 <sup>-</sup>	3013	18009	-2869	[28]			$\pi g^{-1} \nu f_4^2$	15/2 <sup>+</sup>	1647	-8663	319	[51]	
	23/2 <sup>-</sup>	3601	18597	-2281	[28]			$\pi g^{-1} \nu f_6^2$	19/2 <sup>+</sup>			849	<sup>d</sup>	
							$^{146}_{64}\text{Gd}^{\text{b}}$	$\pi h d^{-1}$	6 <sup>-</sup>	3099	3099	-361	[24]	
									7 <sup>-</sup>	2982	2982	-478	[52]	
									8 <sup>-</sup>	3183	3183	-277	[52]	
$^{144}_{62}\text{Sm}^{\text{b}}$	$\pi j^{-2}$	0 <sup>+</sup>	0	8702	-2030	[45]			0 <sup>+</sup>	0	-16322	-1644	[53]	
		2 <sup>+</sup>	1660	10362	-370	[45]			2 <sup>+</sup>	784	-15538	-860	[53]	
		4 <sup>+</sup>	2190	10892	160	[46]			4 <sup>+</sup>	1416	-14906	-228	[53]	
	$\pi g^{-2}$	2 <sup>+</sup>	2800	11502	110	[46]			6 <sup>+</sup>	1811	-14511	167	[53]	
		6 <sup>+</sup>	3308	12010	618	[46]		$^{147}_{65}\text{Tb}^{\text{b}}$	$\pi h^2 d^{-1}$	21/2 <sup>+</sup>	2786	716	-838	[54]
		2 <sup>+</sup>	2423	11125	63	[46]			23/2 <sup>+</sup>	3043	973	-581	[54]	
	$\pi g^{-1} d^{-1}$	3 <sup>+</sup>	<i>2600</i>	<i>11302</i>	<i>240</i>	[3]			25/2 <sup>+</sup>	3190	1120	-434	[54]	
		4 <sup>+</sup>	2588	11290	228	[45]		$^{148}_{65}\text{Tb}^{\text{c}}$	$\pi h \nu f$	8 <sup>+</sup>	406	-9831	-586	[55]
		5 <sup>+</sup>	<i>2620</i>	<i>11322</i>	<i>260</i>	[3]			9 <sup>+</sup>	90	-9741	-496	[54]	
	$\pi h^2 j_0^{-4}$	6 <sup>+</sup>	2323	11025	-37	[45]		$^{149}_{65}\text{Tb}^{\text{b}}$	$\pi h \nu f_0^2$	11/2 <sup>-</sup>	36	-18796	-2212	[56]
8 <sup>(+)</sup>		3651	12353	-5299	[17]			$\pi h \nu f_2^2$	15/2 <sup>-</sup>	823	-18009	-1425	[56]	
10 <sup>(+)</sup>		4221	12923	-4729	[17]			$\pi h \nu f_4^2$	19/2 <sup>-</sup>	1382	-17450	-866	[56]	
								$\pi h \nu f_6^2$	23/2 <sup>-</sup>	1673	-17159	-575	[56]	

TABLE V. (Continued.)

Nucleus	Configuration	Spin	$E_x$	$E$	$\Delta_{\text{int}}$	Ref.
$^{148}\text{Dy}^c$	$\pi h^2$	$8^+$	2833	-3544	268	[57]
		$10^+$	2919	-3458	354	[57]
$^{149}\text{Dy}^b$	$\pi h_{10}^2 \nu f$	$25/2^-$			-250	<sup>d</sup>
		$27/2^-$	2661	-11789	-638	[58]
		$23/2^-$			-432	<sup>d</sup>

<sup>a</sup>Mass excess taken from Blomqvist *et al.* [24].

<sup>b</sup>Mass excess taken from Wapstra *et al.* [26].

<sup>c</sup>Mass excess taken from Rubio *et al.* [25].

<sup>d</sup>Calculated from two-body matrix elements.

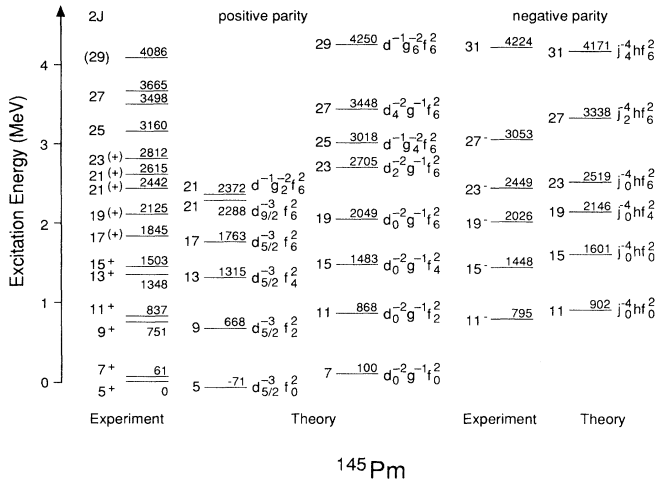


FIG. 10. Comparison between the experimentally observed levels in  $^{145}\text{Pm}$  and the levels from empirical shell model calculations. The abbreviations used are  $d = \pi 2d_{5/2}$ ,  $h = \pi 1h_{11/2}$ ,  $f = \nu 2f_{7/2}$ , and  $j^{-4}$  denotes the  $^{142}\text{Nd}$  core.

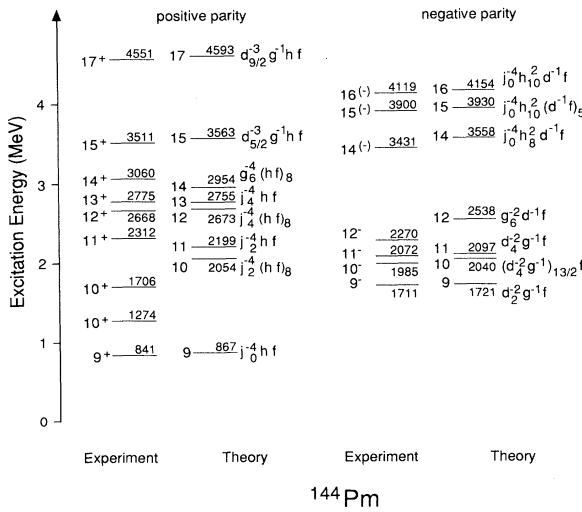


FIG. 11. Comparison between the experimentally observed levels in  $^{144}\text{Pm}$  and the levels from empirical shell model calculations. The abbreviations used are  $d = \pi 2d_{5/2}$ ,  $g = \pi 1g_{7/2}$ ,  $h = \pi 1h_{11/2}$ ,  $f = \nu 2f_{7/2}$ ,  $i = \nu 1i_{13/2}$ , and  $j^{-4}$  denotes the  $^{142}\text{Nd}$  core.

$\pi h_{11/2}$  orbit [30,31,5], which is the unique high spin negative parity proton orbit in this region. The experimentally observed negative parity states in  $^{145}\text{Pm}$  are well reproduced by empirical shell model calculations with configurations of two  $f_{7/2}$  neutrons and one  $h_{11/2}$  proton coupled to a  $^{142}\text{Nd}$  core (the core is denoted by  $j^{-4}$  in Fig. 10). The calculation predicts a  $\frac{31}{2}^-$  state at 4171 keV which probably corresponds to the experimentally observed  $J = \frac{31}{2}$  state at 4224 keV.

The positive parity states in  $^{143}\text{Pm}$  below 2.5 MeV are formed by three proton holes [28] coupled to the  $^{146}\text{Gd}$  core and extend up to the  $[\pi g^{-2}d^{-1}]_{17/2^+}$  yrast level. The observed positive parity states in  $^{145}\text{Pm}$  arise from the coupling of a  $f_{7/2}$  neutron pair to the three hole states in  $^{143}\text{Pm}$ . Configurations of the type  $[\pi^{-3}f^2]$  (where  $\pi$  is either a  $d$  or a  $g$  proton) are observed up to the stretched  $[d^{-1}g_6^{-2}f_6^2]_{29/2^+}$  configuration.

## VII. CONFIGURATIONS FOR $^{144}\text{Pm}$

The structure of the lowest levels in  $^{144}\text{Pm}$  has been discussed [32] in terms of the  $\pi d^{-1}\nu f$  and  $\pi g^{-1}\nu f$  shell model configurations. The proton orbitals  $\pi 2d_{5/2}^{-1}$ ,  $\pi 1g_{7/2}^{-1}$ , and  $\pi 1h_{11/2}$  (abbreviated  $d$ ,  $g$ ,  $h$ ) as well as the neutron orbital  $\nu 2f_{7/2}$  are expected to dominate the configurations of the yrast states in this nucleus since they are of high spin and low excitation energy. Observed and calculated energy levels in  $^{144}\text{Pm}$  for  $J > 8$  are compared in Fig. 11.

The negative parity states in  $^{144}\text{Pm}$  up to spin  $12^-$  are of one-particle-three-hole (1p3h) structure. They arise from the coupling of a neutron to core states in  $^{143}\text{Pm}$ . These core states are dominated [28] by configurations involving  $g_{7/2}$  and  $d_{5/2}$  protons. The valence neutron at low excitation energy in  $^{144}\text{Pm}$  is in the  $2f_{7/2}$  orbit. This is indicated by the pure (more than 95%)  $\nu 2f_{7/2}$  configurations [33] of the  $\frac{7}{2}^-$  ground states in the neighboring nuclei  $^{143}\text{Nd}$  and  $^{145}\text{Sm}$ .

At higher excitation energies, it becomes possible to lift two protons above the  $Z = 64$  shell gap into the  $\pi 1h_{11/2}$  orbit. The  $14^-$ ,  $15^-$ , and  $16^-$  states are assigned  $[j_0^{-4}h^2df]$  configurations with good agreement between observed and calculated energies. We reported this result earlier [34]. While  $\pi h^2$  configurations for nuclei below the  $Z = 64$  shell gap have been suggested in  $N = 82$  isotones [35] this is the first observation of  $\pi h^2$  configurations in an  $N = 83$  isotope for  $Z < 64$ .

The positive parity states in  $^{144}\text{Pm}$  (Fig. 11) are built on the  $9^+$  isomer at 841 keV. This level is assigned a  $[j_0^{-4}hf]_{9^+}$  configuration in agreement with the results from an earlier proton transfer study [32]. Similar  $\pi h_{11/2}$  isomers have been observed in  $^{143}\text{Pm}$  [28] and  $^{145}\text{Pm}$  [36]. This configuration assignment, instead of one in which the  $6_1^-$  state is coupled to an octupole phonon, is further supported by the size of the  $B(E3; 9^+ \rightarrow 6^-)$  reduced transition matrix element which was determined (Table III) to be  $B(E3) = 3.24(71)$  W.u. A single particle estimate (similar to the one for  $^{145}\text{Pm}$  presented

in [5]) predicts a value of  $B(E3; \pi 1h_{11/2} \otimes \nu 2f_{7/2} \rightarrow \pi 2d_{5/2} \otimes \nu 2f_{7/2}) = 3.1$  W.u. In contrast, if the  $9^+$  state was collective in character ( $3^- \otimes \pi 2d_{5/2} \otimes \nu 2f_{7/2}$ ) the strength of the  $E3$  transition would be much larger and comparable to  $B(E3; 0_{g.s.}^+ \rightarrow 3_1^-)$  in the even-even neighbors of  $^{144}\text{Pm}$ , where the values range from to 29 W.u. for  $^{142}\text{Nd}$  to 31 W.u. for  $^{144}\text{Sm}$  [37].

Positive parity states have been observed up to the stretched  $[d^{-3}g^{-1}hf]_{17^+}$  configuration with an average deviation between calculated and observed energies of less than 2% for states above 2 MeV. These are core excited states in  $^{142}\text{Nd}$  coupled to an  $h$  proton and an  $f$  neutron.

The structure of the 1274-keV  $10^+$  state is not understood. The inclusion of octupole phonons into the shell model space has proven useful in the interpretation of high spin states in  $^{146}\text{Eu}$  [2] and might elucidate the origin of this state. The  $10^+$  state at 1274 keV could then arise from the coupling  $[3^- \otimes 7^-]$ , where the  $7^-$  state corresponds to the one at 515 keV. However, the octupole phonon should then also couple to the other low-lying negative parity states and produce larger transition matrix elements than the ones observed.

### VIII. SUMMARY

We have established a high spin decay scheme for  $^{144}\text{Pm}$  with a total of 31 new energy levels up to spin  $20\hbar$  and excitation energies up to 5.8 MeV. Transitions feed-

ing the 841-keV  $9^+$  isomeric state were observed. A measurement of intensities of  $\gamma$ -rays deexciting this state has allowed us to determine the reduced  $B(E3)$  strength for the decay from this state to be  $3.2(7)$  W.u., supporting the interpretation of the  $9^+$  level as a  $[\pi 1h_{11/2} \otimes \nu 2f_{7/2}]$  noncollective state. Our previously published decay scheme for  $^{145}\text{Pm}$  was confirmed and extended up to a tentative spin of  $\frac{33}{2}$  at an excitation energy of 4.7 MeV. The measurement of DCO ratios confirmed previous tentative spin assignments. Configuration assignments to a number of states in  $^{144}\text{Pm}$  and  $^{145}\text{Pm}$  were made on the basis of empirical shell model calculations in a configuration space truncated to the  $\pi 1h_{11/2}$ ,  $\pi 1g_{7/2}^{-1}$ , and  $\pi 2d_{5/2}^{-1}$  protons and the  $\nu 2f_{7/2}$  neutron outside the  $^{146}\text{Gd}$  core in good agreement with the experimental results. It is proposed that three states in  $^{144}\text{Pm}$  involve a  $\pi h^2$  configuration, which had not been observed previously in  $N = 83$  isotones below the  $Z = 64$  shell gap. To confirm these configurations lifetime measurements or single particle transfer experiments will be necessary.

### ACKNOWLEDGMENTS

We thank A. P. Byrne for introducing us to the empirical shell model calculations and R. J. Philpott for illuminating discussions regarding the interpretation of the results. This work was supported by the National Science Foundation and the State of Florida.

- 
- [1] R. F. Casten, D. D. Warner, D. S. Brenner, and R. L. Gill, *Phys. Rev. Lett.* **47**, 1433 (1981).
  - [2] A. Ercan, R. Broda, P. Kleinheinz, M. Piiparinen, R. Julin, and J. Blomqvist, *Z. Phys.* **329**, 63 (1988).
  - [3] M. Piiparinen, Y. Nagai, P. Kleinheinz, M. C. Bosca, B. Rubio, M. Lach, and J. Blomqvist, *Z. Phys. A* **338**, 417 (1991).
  - [4] A. Kuhnert, D. Alber, H. Grawe, H. Kluge, K. H. Maier, W. Reviol, X. Sun, E. M. Beck, A. P. Byrne, H. Hübel, J. C. Bacelar, M. A. Deleplanque, R. M. Diamond, and F. S. Stephens, *Phys. Rev. C* **46**, 484 (1992).
  - [5] T. Glasmacher, D. D. Caussyn, P. D. Cottle, T. D. Johnson, K. W. Kemper, and P. C. Womble, *Phys. Rev. C* **45**, 1619 (1992).
  - [6] A. Gavron, *Phys. Rev. C* **21**, 230 (1980).
  - [7] R. M. Lieder, H. Jäger, A. Neskakis, T. Venkova, and C. Michel, *Nucl. Instrum. Methods* **220**, 363 (1984).
  - [8] PLOTDATA, TRIUMF, Vancouver, B.C. (unpublished).
  - [9] E. der Mateosian and A. W. Sunyar, *At. Data Nucl. Data Tables* **13**, 391 (1974).
  - [10] F. Rösler, H. M. Fries, K. Alder, and H. C. Pauli, *At. Data Nucl. Data Tables* **21**, 109 (1978).
  - [11] K. S. Krane, R. M. Steffen, and R. M. Wheeler, *Nucl. Data Tables* **11**, 351 (1973).
  - [12] J. van Klinken and K. Wisshak, *Nucl. Instrum. Methods* **98**, 1 (1972).
  - [13] M. Ishi, *Nucl. Instrum. Methods* **127**, 53 (1975).
  - [14] Y. Nagai, T. Shibata, S. Nakayama, and H. Ejiri, *Nucl. Phys.* **A282**, 29 (1977).
  - [15] J. Kantele, *Nucl. Instrum. Methods A* **275**, 149 (1989).
  - [16] M. R. MacPhail and R. G. Summers-Gill, *Nucl. Phys.* **A237**, 285 (1975).
  - [17] J. K. Tuli, *Nucl. Data Sheets* **56**, 607 (1989).
  - [18] B. H. Wildenthal, *Phys. Rev. Lett.* **22**, 1118 (1969).
  - [19] M. Ogawa, R. Broda, K. Zell, P. J. Daly, and P. Kleinheinz, *Phys. Rev. Lett.* **41**, 289 (1978).
  - [20] N. R. Walet, P. Stoop, and P. W. M. Glaudemans, *Z. Phys. A* **332**, 9 (1989).
  - [21] I. Talmi, *Rev. Mod. Phys.* **34**, 704 (1962).
  - [22] T. Faestermann, H. Bohn, F. v. Feilitsch, A. W. Sunyar, R. Broda, P. Kleinheinz, and M. Ogawa, *Phys. Lett.* **80B**, 190 (1979).
  - [23] P. Kleinheinz, *Nuovo Cimento A* **81**, 140 (1984).
  - [24] J. Blomqvist, P. Kleinheinz, and P. J. Daly, *Z. Phys. A* **312**, 27 (1983).
  - [25] B. Rubio *et al.*, *Z. Phys. A* **324**, 27 (1986).
  - [26] A. H. Wapstra, G. Audi, and R. Hoekstra, *At. Data Nucl. Data Tables* **39**, 281 (1988).
  - [27] R. D. Lawson, *Theory of the Nuclear Shell Model* (Clarendon Press, Oxford, 1980).
  - [28] H. Prade, L. Käubler, U. Hagemann, H. U. Jäger, M. Kirchbach, L. Schneider, F. Stary, Z. Roller, and V. Paar, *Nucl. Phys.* **A333**, 33 (1980).
  - [29] B. H. Wildenthal, *Phys. Lett.* **29B**, 274 (1969).
  - [30] T. Shibata, Y. Nagai, M. Fujiwara, H. Ejiri, N. Nakanishi, and S. Takeda, *Nucl. Phys.* **A257**, 303 (1976).

- [31] O. Straume, G. Løvholden, and D. G. Burke, *Z. Phys. A* **295**, 259 (1980).
- [32] M. R. Macphail and R. G. Summers-Gill, *Nucl. Phys.* **A263**, 12 (1976).
- [33] Z. Haratym, J. Kownacki, J. Ludziejewski, Z. Sujkowski, L. de Geer, A. Kerek, and H. Ryde, *Nucl. Phys.* **A276**, 299 (1977).
- [34] T. Glasmacher, D. D. Caussyn, P. D. Cottle, T. D. Johnson, K. W. Kemper, M. A. Kennedy, and P. C. Womble, *Z. Phys. A* **345**, 119 (1993).
- [35] R. Wirowski, J. Yan, A. Dewald, A. Gelberg, W. Lieberz, K. P. Schmittgen, A. von der Werth, and P. von Brentano, *Z. Phys. A* **329**, 509 (1988).
- [36] M. Kortelahti, M. Piiparinen, A. Pakkanen, T. Komppa, and R. Komu, *Nucl. Phys.* **A342**, 421 (1980).
- [37] R. H. Spear, *At. Data Nucl. Data Tables* **42**, 55 (1989).
- [38] L. K. Peker, *Nucl. Data Sheets* **63**, 573 (1991).
- [39] H. Prade, J. Döring, W. Enghardt, L. Funke, and L. Käubler, *Z. Phys. A* **328**, 501 (1987).
- [40] S. M. Aziz, P. D. Cottle, K. W. Kemper, M. L. Owens, and S. L. Tabor, *Phys. Rev. C* **41**, 1268 (1990).
- [41] L. K. Peker, *Nucl. Data Sheets* **64**, 429 (1991).
- [42] J. Wrzesinski, A. Clauberg, C. Wesselbord, R. Reinhardt, A. Dewald, K. O. Zell, and P. von Brentano, *Nucl. Phys.* **A515**, 297 (1990).
- [43] D. D. Caussyn, S. M. Aziz, P. D. Cottle, T. Glasmacher, and K. W. Kemper, *Phys. Rev. C* **43**, 2098 (1991).
- [44] L. K. Peker, *Nucl. Data Sheets* **48**, 753 (1986).
- [45] R. Pengo, S. Lunardi, R. Tischler, P. J. Daly, Y. Nagai, R. Broda, and P. Kleinheinz, KFA Jülich, Institut für Kernphysik report, 1978 (unpublished).
- [46] D. Larson, S. M. Austin, and B. H. Wildenthal, *Phys. Rev. C* **9**, 1574 (1974).
- [47] L. K. Peker, *Nucl. Data Sheets* **49**, 46 (1986).
- [48] L. K. Peker, *Nucl. Data Sheets* **41**, 195 (1984).
- [49] R. Kaczarowski, E. G. Funk, and J. W. Mihelich, *Phys. Rev. C* **23**, 2711 (1981).
- [50] G. Lo Bianco, N. Molho, A. Moroni, A. Bracco, and N. Blasi, *J. Phys. G* **7**, 219 (1981).
- [51] R. Julin, A. Pakkanen, M. Piiparinen, B. Rubio, and P. Kleinheinz, JYFL, University of Jyväskylä report, 1985 (unpublished).
- [52] P. Kleinheinz, R. Broda, P. J. Daly, S. Lunardi, M. Ogawa, and J. Blomqvist, *Z. Phys. A* **290**, 279 (1979).
- [53] M. Piiparinen, P. Kleinheinz, S. Lunardi, M. Ogawa, G. de Angelis, F. Soramel, W. Meczynski, and J. Blomqvist, *Z. Phys. A* **337**, 387 (1990).
- [54] R. Broda, M. Behar, P. Kleinheinz, P. J. Daly, and J. Blomqvist, *Z. Phys. A* **293**, 135 (1979).
- [55] L. K. Peker, *Nucl. Data Sheets* **59**, 393 (1990).
- [56] N. C. Singhal, M. W. Johns, and J. V. Thompson, *Can. J. Phys.* **57**, 1959 (1979).
- [57] P. J. Daly, P. Kleinheinz, R. Broda, S. Lunardi, H. Backe, and J. Blomqvist, *Z. Phys. A* **298**, 173 (1980).
- [58] A. M. Stefanini, P. Kleinheinz, and M. R. Maier, *Phys. Lett.* **62B**, 405 (1976).